metals

MDPI

Article

Orientation Relationship of Intergrowth Al_2Fe and Al_5Fe_2 Intermetallics Determined by Single-Crystal X-ray Diffraction

Yibo Liu [1], Changzeng Fan [1,2,*], Bin Wen [1], Zhefeng Xu [1,2], Ruidong Fu [1,2] and Lifeng Zhang [1,3]

[1] State Key Laboratory of Metastable Materials Science and Technology, Yanshan University, Qinhuangdao 066004, China; 202121020059@stumail.ysu.edu.cn (Y.L.); wenbin@ysu.edu.cn (B.W.); zfxu@ysu.edu.cn (Z.X.); rdfu@ysu.edu.cn (R.F.); zhanglifeng@ncut.edu.cn (L.Z.)
[2] Hebei Key Laboratory for Optimizing Metal Product Technology and Performance, Yanshan University, Qinhuangdao 066004, China
[3] School of Mechanical and Materials Engineering, North China University of Technology, Beijing 100144, China
* Correspondence: chzfan@ysu.edu.cn

Abstract: Although the Al_2Fe phase has similar decagonal-like atomic arrangements as that of the orthorhombic Al_5Fe_2 phase, no evidence for intergrowth samples of Al_2Fe and Al_5Fe_2 has been reported. In the present work, the co-existence of Al_2Fe and Al_5Fe_2 phases has been discovered from the educts obtained with a nominal atomic ratio of Al:Fe of 2:1 by arc melting. First, single-crystal X-ray diffraction (SXRD) as well as scanning electron microscope (SEM) equipped with energy-dispersive X-ray spectroscopy (EDX) measurements have been utilized to determine the exact crystal structures of both phases, which are refined to be $Al_{12.48}Fe_{6.52}$ and $Al_{5.72}Fe_2$, respectively. Second, the orientation relationship between Al_2Fe and Al_5Fe_2 has been directly deduced from the SXRD data sets, and the co-existence structure model has been constructed. Finally, four pairs of parallel atomic planes and their unique orientation relations have been determined from the reconstructed reciprocal-space precession images of (0*kl*), (*h*0*l*), and (*hk*0) layers. In addition, one kind of interface atomic structure model is constructed by the orientation relations between two phases, correspondingly.

Keywords: Al_2Fe; Al_5Fe_2; arc melting; single crystal; structural refinement; orientation relationship

Citation: Liu, Y.; Fan, C.; Wen, B.; Xu, Z.; Fu, R.; Zhang, L. Orientation Relationship of Intergrowth Al_2Fe and Al_5Fe_2 Intermetallics Determined by Single-Crystal X-ray Diffraction. *Metals* **2024**, *14*, 337. https://doi.org/10.3390/met14030337

Academic Editor: Jean-Louis Bobet

Received: 27 February 2024
Revised: 9 March 2024
Accepted: 14 March 2024
Published: 15 March 2024

1. Introduction

Similar to the Al-Mn system, diverse complex intermetallics in the binary Al-Fe system have been discovered, including quasiperiodic and periodic quasi-crystalline approximate phases [1,2]. Among them, the Al_2Fe and Al_5Fe_2 phases have been extensively studied [3–7]. Studies on the crystal structure of the Al_2Fe phase can be traced back to half a century ago. In 1973, Corby et al. [8] studied the crystal structure of Al_2Fe for the first time using the anomalous dispersion method. The refined composition of the phase is $Al_{11}Fe_7$ with space group *P*1; There are three Al/Fe co-occupying atoms in the unit cell. The lattice parameters are determined to be a = 4.878 (1) Å, b = 6.461 (2) Å, c = 8.800 (3) Å, α = 91.75 (5)°, β = 73.27 (5)°, γ = 96.89 (3)°. In 1978, Bastin et al. [9] investigated the crystal structure of Al_2Fe using the Weissenberg technique. The authors consider the unit cell of Al_2Fe can be described as an A-centered pseudo-monoclinic cell with a = 7.594 Å, b = 16.886 Å, c = 4.863 Å, α = 89.55°, β = 122.62°, γ = 90.43°. Due to the inconsistency of the above two research results, Chumak et al. [10] have re-determined the crystal structure of Al_2Fe again by single-crystal X-ray diffraction method in 2010. The refined composition was $Al_{12.59}Fe_{6.41}$ with space group $P\bar{1}$. There are two Al/Fe co-occupying atoms in the unit cell, and the lattice parameters are a = 4.8745 (6) Å, b = 6.4545 (8) Å, c = 8.7361 (10) Å, α = 87.930 (9)°, β = 74.396 (9)°, γ = 83.062 (9)°. For the crystal structure of Al_5Fe_2. Schubert et al. [11] first determined the crystal structure of the Al_5Fe_2 phase by X-ray powder diffraction method in 1953. They consider the phase to have *Cmcm* space group and consists of three independent atoms, including a vacancy atom Al1 with an occupancy of 0.7. The cell parameters are

a = 7.675 Å, b = 6.403 Å, c = 4.203 Å, α = 90°. In 1994, Burkhardt et al. [12] re-determined the fine crystal structure of this phase by the single-crystal X-ray diffraction method. They proposed that this phase has two vacant atoms, namely Al1 and Al2 atoms, with the site of occupation factors (S.O.F) of 0.32 and 0.24, respectively. Furthermore, several studies have shown that the Al_5Fe_2 phase has an ordered cryogenic phase [13–16].

As aforementioned, the crystal structure models of Al_2Fe and Al_5Fe_2 phases have been studied extensively; however, there are no reports on the co-existence of the two phases. Mihalkovič et al. [17] studied the structure and stability of Al_2Fe and Al_5Fe_2 phases by first-principles calculations. Hirata et al. [18] studied the crystal structure of Al_2Fe and Al_5Fe_2 phases and found that the crystal structure of the two phases has a similar decagonal-like atomic arrangement. Romero-Romero et al. [19] studied the structural stability of Al_2Fe and Al_5Fe_2 phases by the high-energy ball-milling method. They found that the Al_2Fe phase underwent a phase transition and transformed into the Al_5Fe_2 phase after 10 h of high-energy ball milling.

In the present work, samples with nominal Al_2Fe composition were prepared using the arc melting method, and the co-existence of the Al_2Fe phase and Al_5Fe_2 phase in the educts was discovered by analyzing the SXRD data sets. Second, we solved and refined the crystal structures of the two phases separately and obtained the orientation relationship of the two phases in real space by comparing their orientation matrix in the reciprocal space. Finally, concerning the vitally important role played by interfaces for industrial applications [20,21], the parallel atomic planes between the coexisting phases were analyzed, and one preferential interface was constructed by referring to the reconstructed reciprocal-space precession images.

2. Materials and Methods

High-purity aluminum (2.457 g) and iron (2.543 g) powders, according to the atomic ratio of 2:1, were pressed into blocks and then melted in a vacuum furnace for 4 cycles to ensure a uniform composition. The sintered block was broken into small pieces, and a cuboid-shaped fragment with a size of 0.08 × 0.06 × 0.03 mm^3 was selected and mounted on a thin glass fiber for SXRD measurements. Diffraction measurements were carried out with a four-circle single-crystal X-ray diffractometer (Bruker D8 Venture, Bruker AXS GmbH, Karlsruhe, Germany). Two SEM and EDX tests have been conducted on the sample. In the first test, the electron microscope Hitachi S-3400N type equipped with EDX (EDAX Inc., Mahwah, NJ, USA) was used, and in the second test, the electron microscope ZEISS Sigma 300 type equipped with EDX (Oxford, UK) was used.

All data sets from SXRD are processed by the APEX3 program [22], including indexing, integration, scaling, absorption correction [23], space group determination, structural solving, and refinement [24,25]. The structural models are drawn with the Diamond program [26]. The building clusters of the studied phases are analyzed by the ToposPro package [27].

3. Results

3.1. Single-Crystal XRD Patterns

The diffraction points in the reciprocal space of the whole sample collected by 10 runs of the single-crystal XRD measurements are illustrated in Figure 1. As can be seen from Figure 1, these diffraction points can be clearly divided into two different data sets, implying two independent different phases. In the following, the two data sets will be analyzed separately in the reciprocal space. It needs to be noted that the single-crystal X-ray diffraction measurements on the sample include a total of 10 runs, and a total of 4793 diffraction points were harvested with the criteria of $I/\sigma(I)$ equals 3 in the reciprocal space when indexing the phases. Among these 4793 diffraction points, there are 2984 diffraction points belong to the Al_2Fe phase, 1032 diffraction points belong to the Al_5Fe_2 phase, and the remaining 777 diffraction points belong to anomalous phases, either an amorphous phase or some very tiny crystalline phases, which cannot be indexed to de-

termine a unit cell. We have also conducted a Phi360 test (with the sample rotating around the psi axis) on the sample by the single-crystal X-ray diffraction diffractometer, which is equivalent to XRD powder diffraction (see Figure S1 of the Supplementary Material).

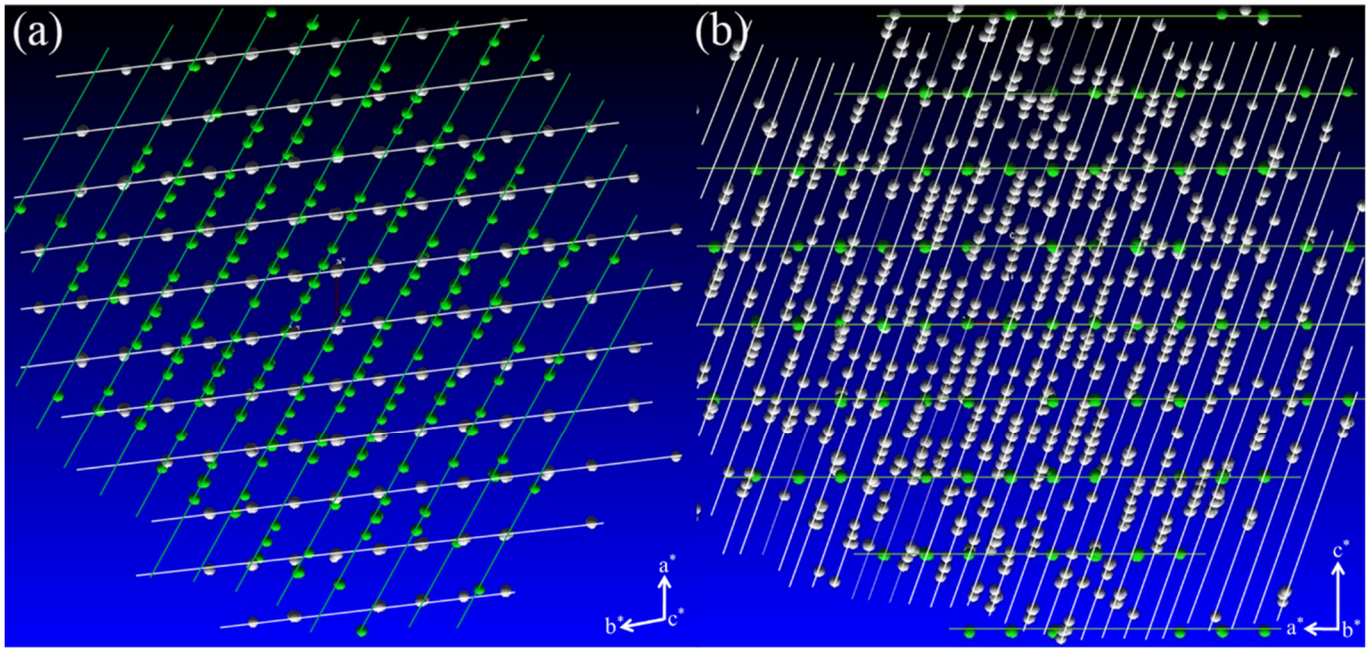

Figure 1. Diffraction points in the reciprocal space of the whole sample projected along different directions. The data set in white and green color indicates the Al_2Fe phase and the Al_5Fe_2 phase, respectively: (**a**) Projection along the c*-axis of the Al_2Fe phase; (**b**) Projection along the b*-axis of the Al_5Fe_2 phase.

Figures 2 and 3 illustrate the diffraction patterns of the Al_2Fe and Al_5Fe_2 phases projected in three axes, along with their crystal structures, respectively. It can be seen that the diffraction points in the reciprocal space are arranged quite neatly for both phases. The first data set (indicated as white color in Figure 1) is indexed to be a = 4.86 Å, b = 6.44 Å, c = 8.74 Å, α = 87.88°, β = 74.47°, γ = 83.06°, in accordance with those of the Al_2Fe phase as shown in Figure 2. The second data set (indicated as green color in Figure 1) is indexed to be a = 7.63 Å, b = 6.41 Å, c = 4.20 Å, $\alpha = \beta = \gamma$ = 90°, in accordance with those of the Al_5Fe_2 phase as shown in Figure 3. The cell parameters of the Al_2Fe and Al_5Fe_2 phases are detailed in Table 1.

Table 1. Crystallographic and experimental data of $Al_{12.48}Fe_{6.52}$ and $Al_{5.72}Fe_2$.

Chemical Formula	**$Al_{12.48}Fe_{6.52}$**	**$Al_{5.72}Fe_2$**
a, b, c/Å	4.8569 (5), 6.4389 (7), 8.7323(10)	7.635 (3), 6.392 (2), 4.2007 (14)
α, β, γ/°	87.873 (4), 74.463 (4), 83.060 (4)	90, 90, 90
V/Å^3	261.18 (5)	205.01 (12)
Z	4	4
Space group	$P\bar{1}$	*Cmcm*
Crystal system	Triclinic	Orthorhombic
Diffractometer	Bruker D8 Venture Photon 100 COMS	
Monochromator	Graphite	
T_{meas}/K	300 (2)	
Radiation	Mo-Kα, λ = 0.71073 (Å)	
Scan mode	φ and ω scan	
Time per step/s	3	
Absorption correction	Multi-scan	

Table 1. *Cont.*

Chemical Formula	**$Al_{12.48}Fe_{6.52}$**	**$Al_{5.72}Fe_2$**
F (000)	332	253
θ range/°	2.421~27.571	4.158~24.997
μ/mm^{-1}	9.803	8.088
No. measured reflections	7202	283
No. unique reflections	1210	100
No. observed reflections (I > 2σ (I))	907	76
No. reflections used in refinement	1210	100
No. parameters used in refinement	89	19
Reflection range	$-6 \leq h \leq 6$, $-8 \leq k \leq 8$, $-11 \leq l \leq 11$	$-6 \leq h \leq 9$, $-6 \leq k \leq 7$, $-4 \leq l \leq 4$
R_{int}	0.0957	0.0567
R (σ)	0.0692	0.0915
Final R indices (Fobs > 4σ (Fobs))	$R_1 = 0.0543$, $\omega R_2 = 0.1044$	$R_1 = 0.0363$, $\omega R_2 = 0.0844$
R indices (all data)	$R_1 = 0.0797$, $\omega R_2 = 0.1044$	$R_1 = 0.0597$, $\omega R_2 = 0.0844$
Goodness of fit	1.057	1.017

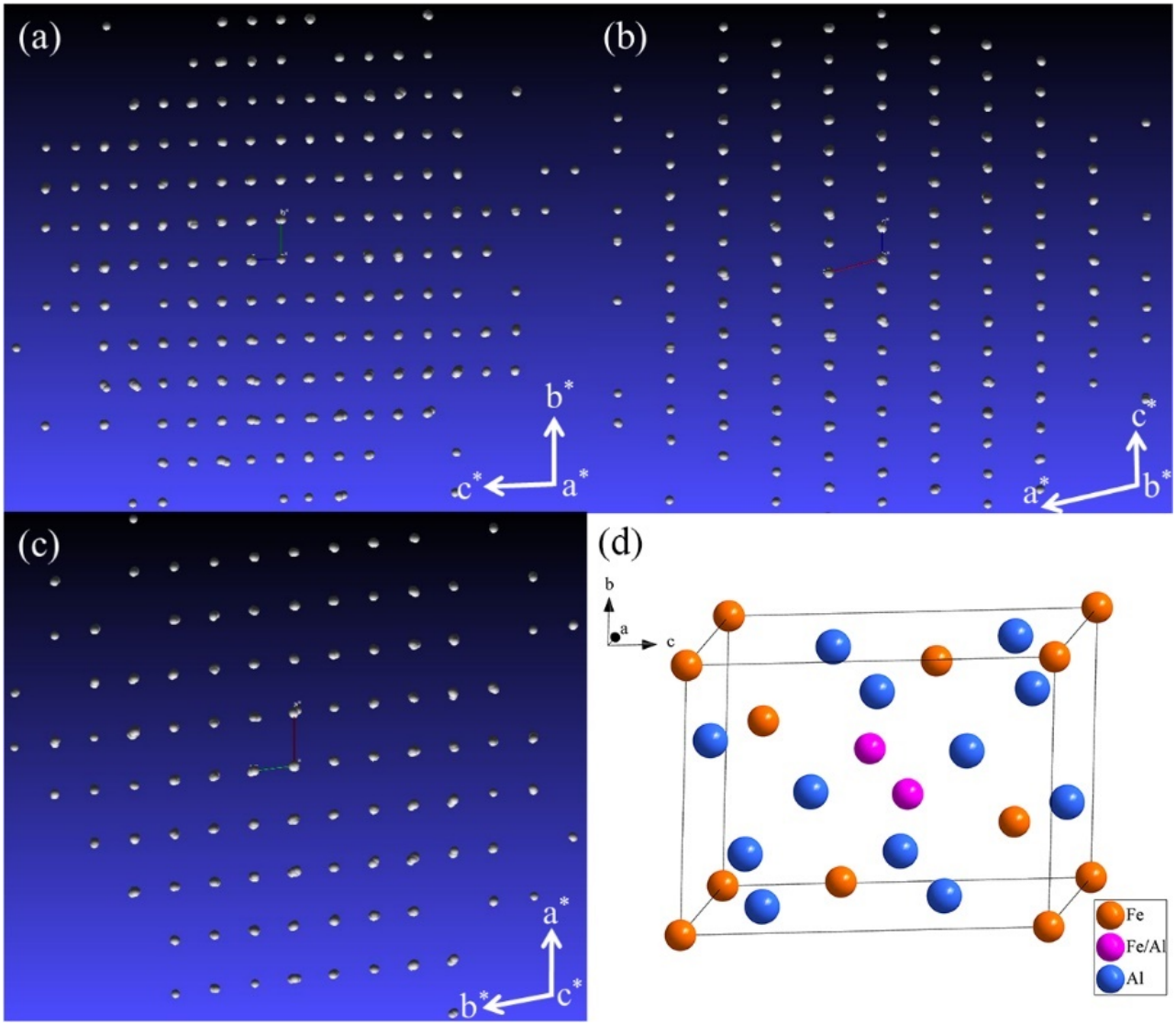

Figure 2. The diffraction patterns of the Al_2Fe and its crystal structure: (**a**) Projection along the a*-axis; (**b**) Projection along the b*-axis; (**c**) Projection along the c*-axis; (**d**) Crystal structure of Al_2Fe phase.

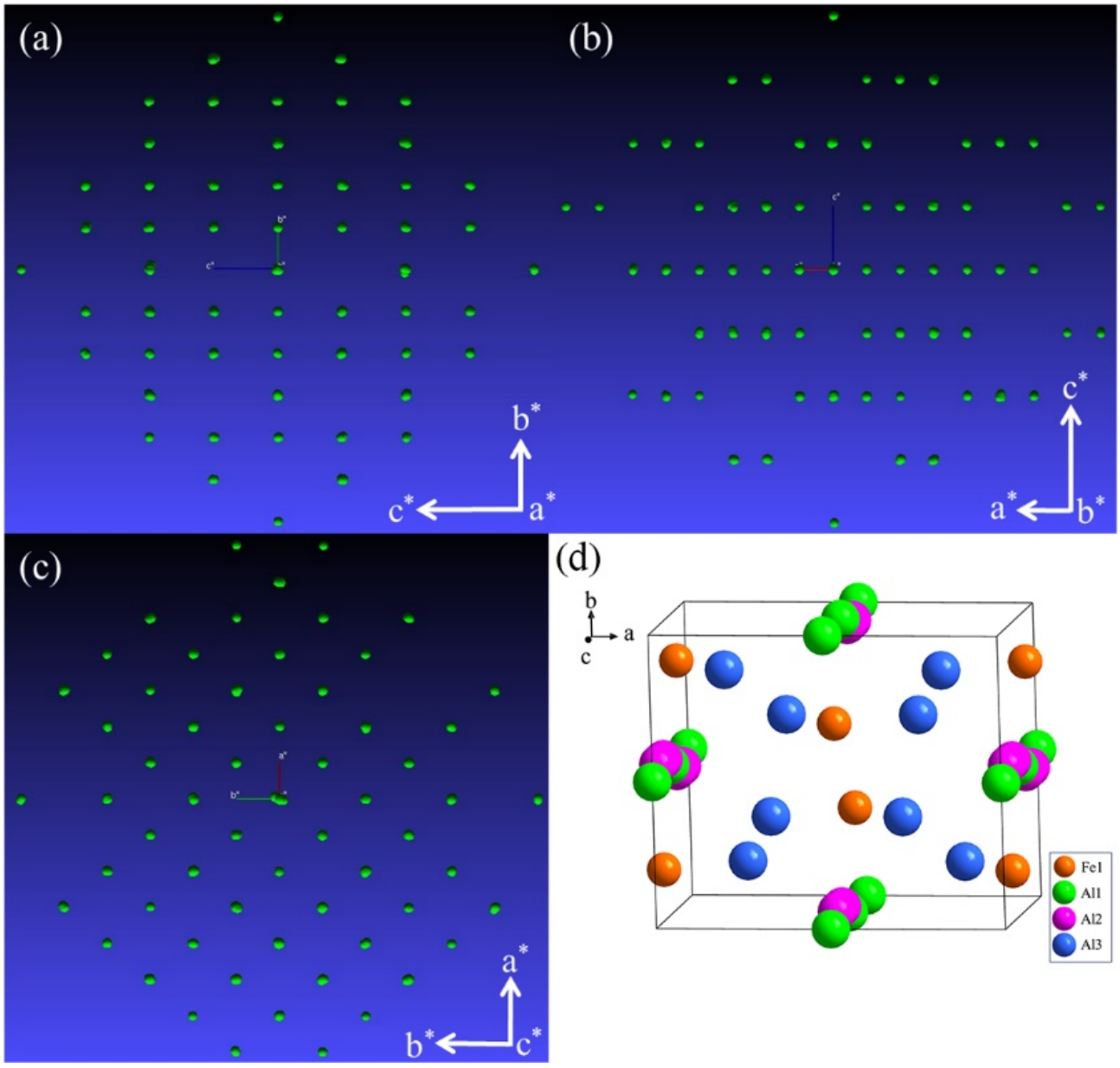

Figure 3. The diffraction patterns of the Al_5Fe_2 and its crystal structure: (**a**) Projection along the a*-axis; (**b**) Projection along the b*-axis; (**c**) Projection along the c*-axis; (**d**) Crystal structure of Al_5Fe_2 phase.

3.2. The Refinement of Al_2Fe Phase and Al_5Fe_2 Phase

Detailed crystal data, data collection, and structure refinement details are summarized in Table 1. For the Al_2Fe phase, as the residual electron density around the Fe4 atom is too large, thus it is designated as a disordered atom, and the PART instruction (means to divide disordered atoms into two or more groups, each representing a disordered component) is used to separate it to Fe4A atom and Al4B atom. The S.O.F for Fe4A and Al4B atoms is 0.758 and 0.242, respectively. All the remaining atoms are completely occupied, and the chemical formula was refined to $Al_{12.48}Fe_{6.52}$. The final crystallographic parameter R_1 is 0.0543, ωR_2 is 0.1044 ($F_{obs} > 4\sigma$ (F_{obs})), and goodness of fit S is 1.057. During the structural refinement of Al_5Fe_2 phase, it is found that it is more reasonable for Al1 and Al2 atoms to be refined in the form of vacancy atoms with the S.O.F of the Al1 atom to be 0.50 while that of the Al2 atom to be 0.18, resulting the final refined chemical formula to be $Al_{5.72}Fe_2$. The

final crystallographic parameter R_1 is 0.0363, ωR_2 is 0.0844 ($F_{obs} > 4\sigma$ (F_{obs})), and goodness of fit S is 1.017. All the parameters meet the requirements of international crystallography for the rationalization of the crystal structure.

Table 2 shows detailed information about the atomic occupancy of the $Al_{12.48}Fe_{6.52}$ phase, where U_{eq} is the equivalent isotropic temperature factor and Occ. is the site of occupation factors of atoms. It can be seen that there are two disordered (co-occupying) atoms in this structure, named the Fe4A atom and the Al4B atom. These two atoms occupy the same position with S.O.F of 0.758 and 0.242 for Fe4A and Al4B, respectively. When comparing the present refined crystal structure model with the previously reported Al_2Fe phase as refined to be $Al_{12.59}Fe_{6.41}$ determined in 2010 [10], one can find that they agree with each other quite well except for the slightly different S.O.F for the co-occupied position. In the previous model, the S.O.F is 0.705 and 0.295 for Fe4A and Al4B, respectively, while in the present one, the ratio of S.O.F between Fe4A and Al4B is much closer to 3:1.

Table 2. Fractional atomic coordinates and equivalent isotropic displacement parameters ($Å^2$) of $Al_{12.48}Fe_{6.52}$.

Label	Site	*x*	*y*	*z*	Occ.	U_{eq}
Fe1	2*i*	0.1425 (3)	0.15847(19)	0.41690 (14)	1	0.0066 (3)
Fe2	2*i*	0.2296 (3)	0.3508 (2)	0.87452 (15)	1	0.0102 (3)
Fe3	1*a*	0.000000	0.000000	0.000000	1	0.0083 (4)
Fe4A	2*i*	0.1640 (3)	0.4744 (2)	0.59039 (18)	0.758 (12)	0.0115 (5)
Al4B	2*i*	0.1640 (3)	0.4744 (2)	0.59039 (18)	0.242 (12)	0.0115 (5)
Al1	2*i*	0.4915 (6)	0.0106 (4)	0.1650 (3)	1	0.0129 (6)
Al2	2*i*	0.0430 (6)	0.1158 (5)	0.7096 (3)	1	0.0135 (6)
Al3	2*i*	0.5994 (6)	0.1853 (4)	0.5253 (3)	1	0.0140 (6)
Al4	2*i*	0.0150 (6)	0.2924 (4)	0.1691 (3)	1	0.0123 (6)
Al5	2*i*	0.3101 (5)	0.6635 (4)	0.0349 (3)	1	0.0079 (6)
Al6	2*i*	0.4198 (6)	0.4451 (4)	0.2983 (3)	1	0.0102 (6)

In the following, the building units of the Al_2Fe phase have been analyzed by applying the nanocluster method as integrated into the ToposPro software (Version 5.5.2.0, programed by V. A. Blatov and A. P. Shevchenko). One finds that the crystal structure model can be described by two cluster types: Fe3 (1) (1@12) and Al6 (1) (1@13). Among them, the Fe3 (1) (1@12) cluster is an icosahedral cluster with the Fe3 atom as the center, and the Al6 (1) (1@13) is a 21-dihedral cluster with an Al6 atom located at the center. Figure 4a shows the centers of the aforementioned different clusters in the unit cell. As shown in Figure 4b, the Al6 (1) (1@13) clusters are connected with Fe3 (1) (1@12) clusters either by common vertex, edge, or plane, while two Al6 (1) (1@13) clusters are connected with a common plane. Two Fe3 (1) (1@12) clusters along the a-axis are also connected by a common edge. Figure 5 shows the environments of Fe3 and Al6 atoms. It can be seen that the Fe3 atom is surrounded by 12 atoms while the Al6 atom is surrounded by 13 atoms.

Table 3 shows detailed information on the $Al_{5.72}Fe_2$ phase. There are two vacancy atoms, namely the Al1 atom and the Al2 atom, and the occupying factor of the Al1 atom is 0.50 (10), and that of the Al2 atom is 0.18 (5). By comparing the present work with the $Al_{5.4}Fe_2$ obtained by Schubert et al. [11], the present model contains an additional Al atom at the 8*f* position. Compared with the $Al_{5.6}Fe_2$ determined by Burkhardt et al. in 1994 [12], Al1 and Al2 atoms in the present $Al_{5.72}Fe_2$ phase have slightly different S.O.F. The occupancy of Al atoms at 4*b* and 8*f* site in the previous $Al_{5.6}Fe_2$ phase is 0.32 and 0.24, while the occupancy of Al atoms at 4b and 8f in the $Al_{5.72}Fe_2$ phase is 0.50 and 0.18, respectively, in the present work. It is also necessary to note that Okamoto et al. [14] have constructed Al_8Fe_3 and Al_7Fe_3 phases with the $Al_{5.6}Fe_2$ phase as the basic unit. As the difference in the occupancy of vacant Al atoms in the present $Al_{5.72}Fe_2$ phase and the previous $Al_{5.6}Fe_2$ phase, it is believed that this may lead to the emergence of some modified Al_8Fe_3 and Al_7Fe_3 structure models. (See Supplementary Materials for details).

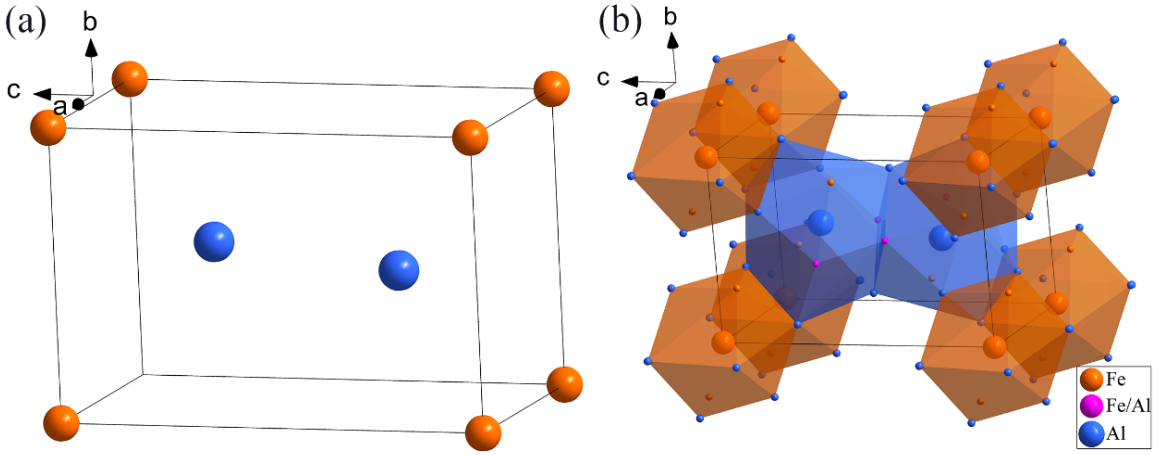

Figure 4. Cluster assembly in Al_2Fe phase cell: (**a**) The central atom of the cluster; (**b**) Cluster assembly model.

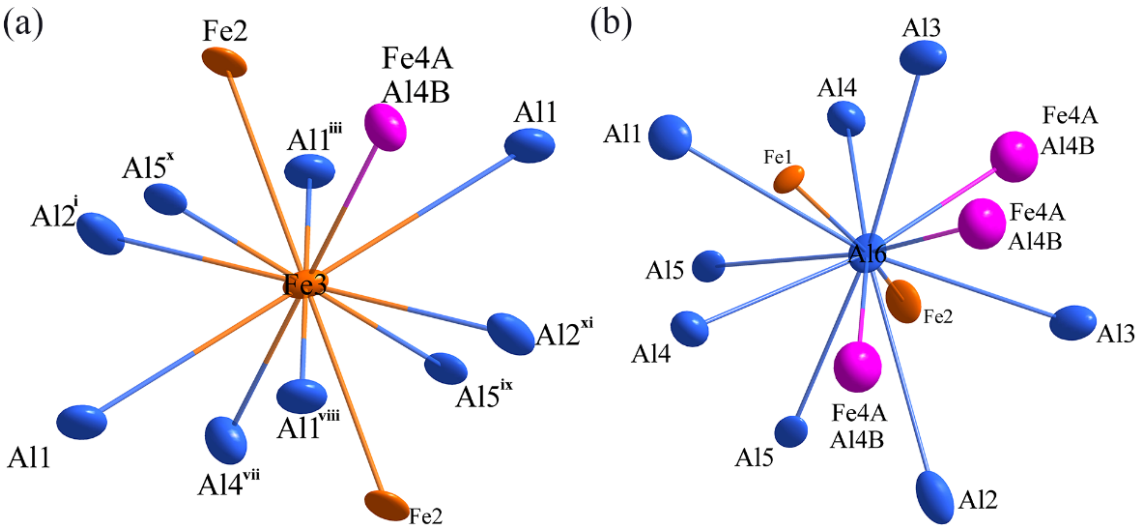

Figure 5. Environment diagram of atoms: (**a**) Fe3 atom; (**b**) Al6 atom. Symmetry codes: (i) $-x, -y, -z+1$; (iii) $x-1, y, z$; (vii) $-x, -y, -z$; (viii) $-x+1, -y, -z$; (ix) $-x, -y+1, -z$; (x) $x, y-1, z$; (xi) $x, y, z-1$.

Table 3. Fractional atomic coordinates and equivalent isotropic displacement parameters ($Å^2$) of $Al_{5.72}Fe_2$ phase.

Label	Site	*x*	*y*	*z*	Occ.	U_{eq}
Fe1	4*c*	0.000000	0.8279 (4)	0.250000	1	0.0081 (8)
Al1	4*b*	0.000000	0.500000	0.000000	0.50 (10)	0.03 (2)
Al2	8*f*	0.000000	0.537 (6)	0.81 (4)	0.18 (5)	0.03 (2)
Al3	8*g*	0.1888 (4)	0.1454 (6)	0.250000	1	0.0158 (12)

Then, we focus on the crystallographic feature of the $Al_{5.72}Fe_2$ phase. Figure 6a shows the $2 \times 2 \times 2$ supercell of $Al_{5.72}Fe_2$ projected along the [001] direction. The Al1 and Al2 atoms (designated in green and pink color, respectively) are surrounded by a hole composed of eight Al3 atoms and two Fe1 atoms (designated in blue and orange color, respectively). The distance between Al1 and Al2 is only 0.7982 Å, confirming that both have to be partially occupied atoms. Figure 6b shows a projection of the $Al_{5.72}Fe_2$ supercell along the direction [100], where one can see that the Al1 and Al2 atoms are alternatively distributed along the c-axis.

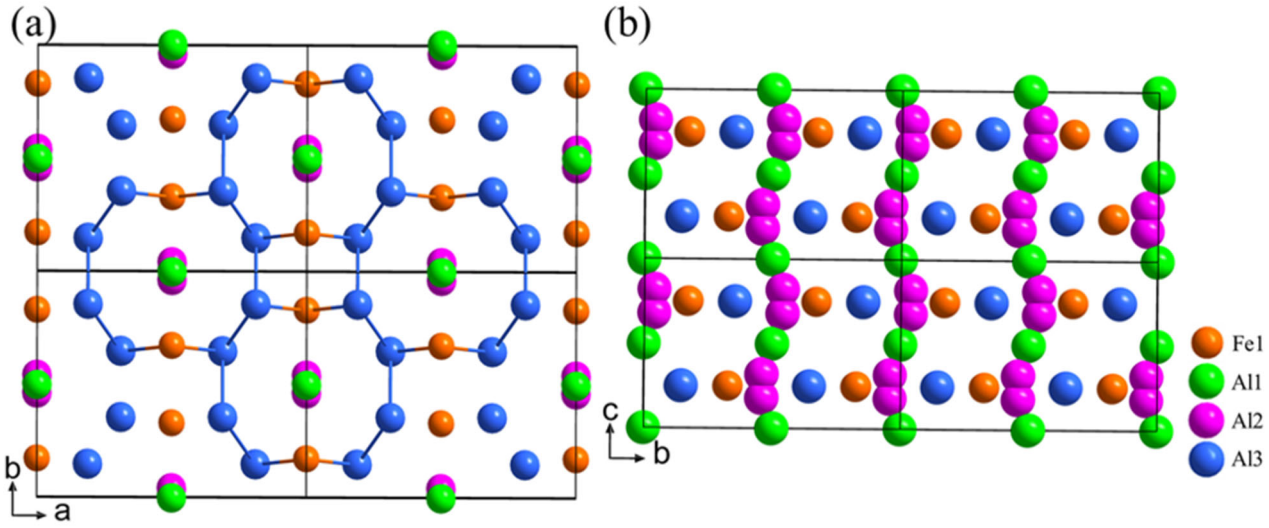

Figure 6. Projection of the $Al_{5.72}Fe_2$ supercell along directions: (**a**) [001] and (**b**) [100].

It was found that the unit cell of $Al_{5.72}Fe_2$ is composed of four twisted icosahedrons, as shown in Figure 7. The icosahedron takes an Al1 atom as its center, and each icosahedron is connected by a common edge. As described in Section 3.1, the structural model of $Al_{12.48}Fe_{6.52}$ can also be described by icosahedron. Such common structural features could be the reason for their growing together.

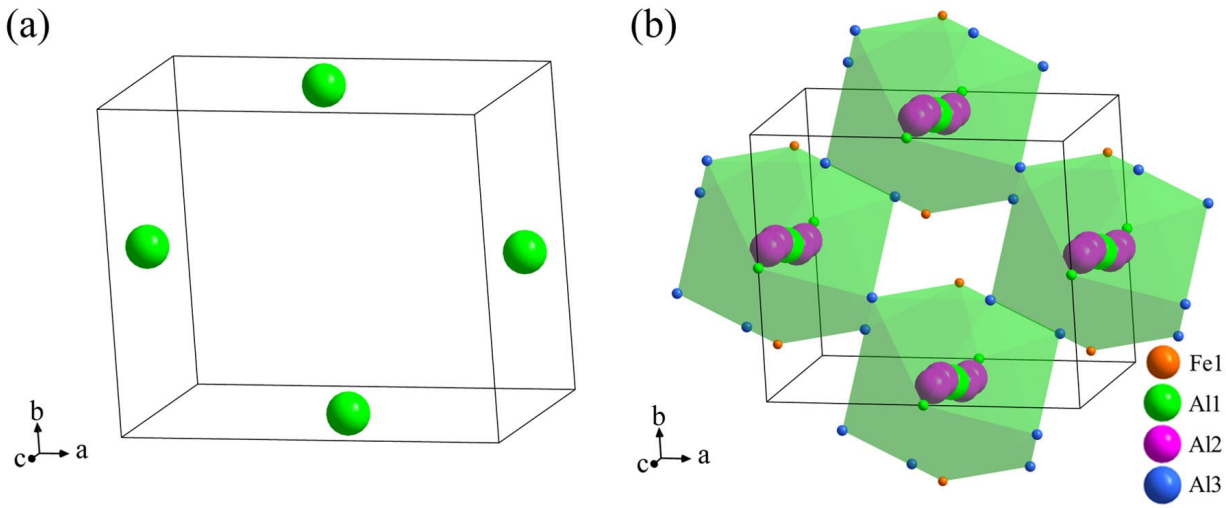

Figure 7. Cluster assembly in $Al_{5.72}Fe_2$ phase cell: (**a**) The central atom of the cluster; (**b**) Cluster assembly model.

3.3. Structure Models for Intergrowth $Al_{12.48}Fe_{6.52}$ Phase and $Al_{5.72}Fe_2$ Phase in Real Space

In the above section, we have explained the crystal structure of the $Al_{12.48}Fe_{6.52}$ phase and $Al_{5.72}Fe_2$ phase, respectively. In this section, the orientation model of real space will be constructed through the orientation matrix of these two phases in reciprocal space. Please refer to Appendix A for the specific construction method of structure models for intergrowth $Al_{12.48}Fe_{6.52}$ phase and $Al_{5.72}Fe_2$ phase in real space. First, the orientation matrix of two phases in reciprocal space is obtained by APEX3 software (v2018.1-0), and then the orientation relationship of two phases in real space is obtained by the basic correspondence between reciprocal space and real space [28], and the orientation model of two-phase single cell edges in real space is obtained. As shown in Figure 8a, the black and red frames show the cell edges of the $Al_{12.48}Fe_{6.52}$ and $Al_{5.72}Fe_2$ phases, respectively. Finally, the final orientation model is obtained by adding atoms to the two-phase cell edges.

In Figure 8b, the left shows the unit cell of $Al_{12.48}Fe_{6.52}$, and the right shows the unit cell of $Al_{5.72}Fe_2$. It is interesting to find that the angle between the crystal plane of $Al_{12.48}Fe_{6.52}$ (001) and the crystal plane of $Al_{5.72}Fe_2$ (100) is 63.35°.

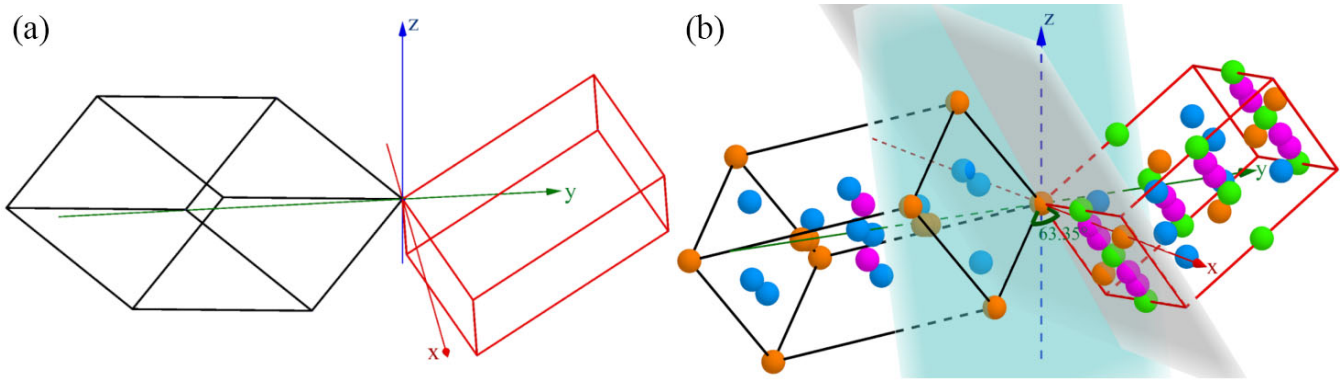

Figure 8. Oriented structural models described with cell edges (**a**) and unit cell (**b**) for $Al_{12.48}Fe_{6.52}$ and $Al_{5.72}Fe_2$ phases.

3.4. Interfaces between $Al_{12.48}Fe_{6.52}$ Phase and $Al_{5.72}Fe_2$ Phases

In the previous section, we obtained the oriented structural models of $Al_{12.48}Fe_{6.52}$ and $Al_{5.72}Fe_2$. However, the orientation of the interfaces between the two phases and the arrangement of atoms inside the interfaces are still elusive. In this section, we will focus on solving such issues by investigating the synthesized precession images from the SXRD data sets, as shown in Figure 9. Figure 9a–c represent the precession images of the (0*kl*), (*h*0*l*), and (*hk*0) planes from the $Al_{12.48}Fe_{6.52}$ phase, while Figure 9d–f represent the precession images of the (0*kl*), (*h*0*l*) and (*hk*0) planes from the $Al_{5.72}Fe_2$ phase. In Figure 9a–c, the green and blue circles represent the crystal planes of the $Al_{12.48}Fe_{6.52}$ phase and the $Al_{5.72}Fe_2$ phase, respectively. The precession images are constructed with a thickness of 0.05 $Å^{-1}$ and a resolution of 0.80 Å. While in Figure 9d–f, the green and blue circles represent the crystal planes of the $Al_{5.72}Fe_2$ phase and the $Al_{12.48}Fe_{6.52}$ phase, respectively, the precession images are constructed with a thickness of 0.03 $Å^{-1}$ and a resolution of 0.80 Å. It needs to be emphasized that the "reconstructed precession images" are obtained by the APEX3 program, where the Synthesize Precession Images plug-in provides an undistorted view of layers of the reciprocal lattice. It generates simulated precession images by finding the appropriate pixels in a series of frames.

The orientation relationship of the $Al_{12.48}Fe_{6.52}$ and $Al_{5.72}Fe_2$ phases expressed by a pair of crystal planes can be observed directly from Figure 9. Those diffraction points from the two phases overlap, which means the crystal planes they represent are parallel with each other. To summarize, four orientation relationships named OR1, OR2, OR3, and OR4 can be obtained by analyzing the (0*kl*), (*h*0*l*), and (*hk*0) planes of the $Al_{12.48}Fe_{6.52}$ phase and the (*hk*0) planes of the $Al_{5.72}Fe_2$ phase are shown in Table 4.

Table 4. Four crystallographic orientation relationships at the interface of $Al_{12.48}Fe_{6.52}$ and $Al_{5.72}Fe_2$.

	$[uvw]_{Al12.48Fe6.52}//[uvw]_{Al5.72Fe2}$	$(hkl)_{Al12.48Fe6.52}//(hkl)_{Al5.72Fe2}$
OR1	$[010]_{Al12.48Fe6.52}//[\bar{3}726]_{Al5.72Fe2}$	$(308)Al_{12.48}Fe_{6.52}//(\bar{7}\bar{3}0)_{Al5.72Fe2}$
OR2	$[010]_{Al12.48Fe6.52}//[\bar{3}726]_{Al5.72Fe2}$	$(308)\ Al_{12.48}Fe_{6.52}//(\bar{7}\bar{3}0)_{Al5.72Fe2}$
OR3	$[001]_{Al12.48Fe6.52}//[794]_{Al5.72Fe2}$	$(350)\ Al_{12.48}Fe_{6.52}//(\bar{4}\bar{4}2)_{Al5.72Fe2}$
OR4	$[\bar{5}\bar{9}2]_{Al12.48Fe6.52}//[001]_{Al5.72Fe2}$	$(313)\ Al_{12.48}Fe_{6.52}//(\bar{5}10)_{Al5.72Fe2}$

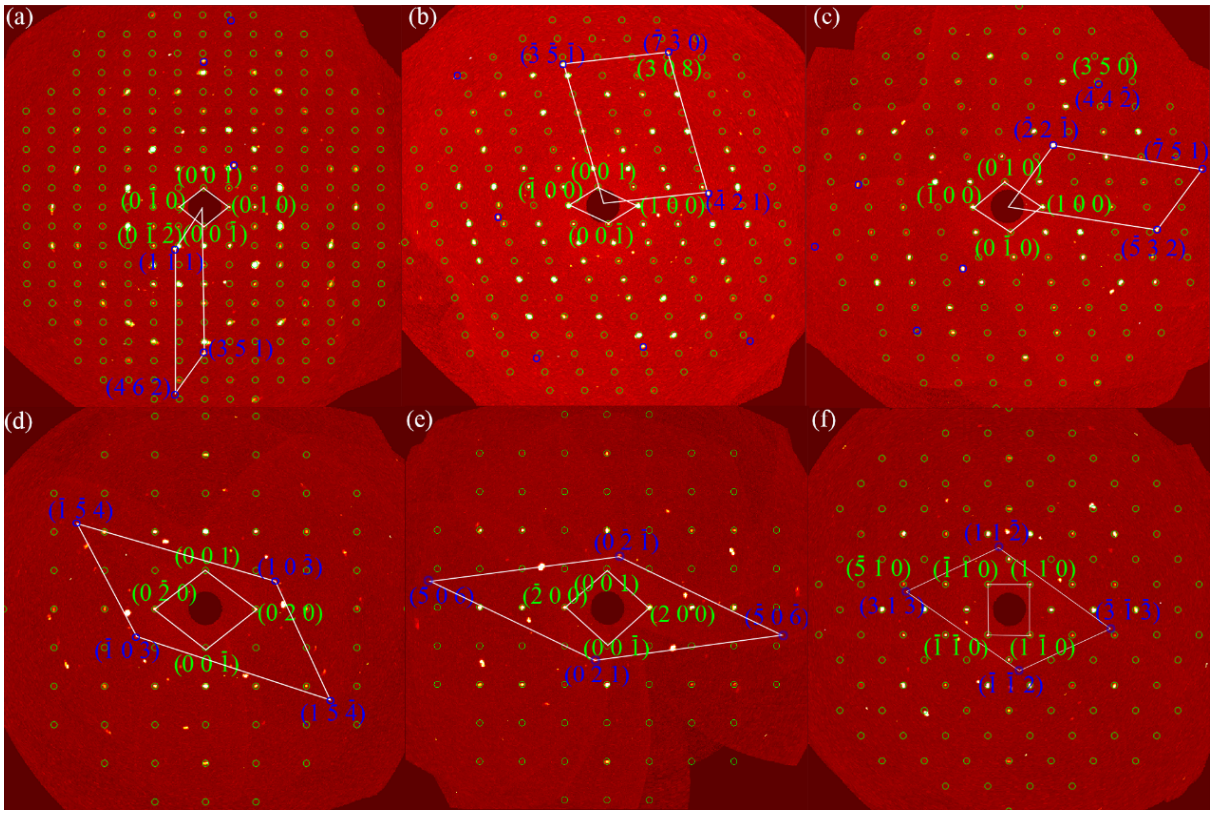

Figure 9. The precession images of intergrowth crystals: (**a**) $Al_{12.48}Fe_{6.52}$ (0*kl*), (**b**) $Al_{12.48}Fe_{6.52}$ (*h*0*l*), (**c**) $Al_{12.48}Fe_{6.52}$ (*hk*0), (**d**) $Al_{5.72}Fe_2$ (0*kl*), (**e**) $Al_{5.72}Fe_2$ (*h*0*l*), (**f**) $Al_{5.72}Fe_2$ (*hk*0).

As mentioned above, we have identified four crystallographic orientation relationships between the $Al_{12.48}Fe_{6.52}$ and $Al_{5.72}Fe_2$ phases from Figure 9. According to the symmetry principle of crystallography, there are usually multiple variants corresponding to a set of experimentally determined orientation relationships. It is necessary to judge if the four crystallographic orientation relationships observed in this experiment are equivalent. In the following, the matrix method is used to analyze and discuss the experimental results.

A detailed explanation of the matrix method can be found in Appendix B. Through this method, we obtain the conversion matrix between the four orientation relationships, as shown in the following Table 5, where matrix B represents the conversion matrix between crystal directions and matrix A represents the conversion matrix between crystal planes. The absolute values of the elements in the conversion matrices corresponding to the four orientation relationships are different, so it is confirmed that they are four independent orientation relationships.

Furthermore, a preliminary interface model of these interface relationships was built. The OR1 orientation relationship: $[100]_{Al12.48Fe6.52}//[\bar{2}11]_{Al5.72Fe2}$, $(0\bar{1}\bar{2})_{Al12.48Fe6.52}//(111)_{Al5.72Fe2}$ is used as an example. For the $(0\bar{1}\bar{2})_{Al12.48Fe6.52}$ surface model, as shown in Figure 10a, the *u* and *v* directions are parallel to $[\bar{2}21]$ and [100], respectively. At this time, the lattice parameters of the surface of $Al_{12.48}Fe_{6.52}$ $(0\bar{1}\bar{2})$ are u = 17.685 Å, v = 4.857 Å, θ = 59.669°. For the surface model of $(111)_{Al5.72Fe2}$, as shown in Figure 10b, the *u* and *v* directions are parallel to $[\bar{1}\bar{3}2]$ and $[\bar{2}\bar{1}1]$, respectively. The lattice parameters of the surface of $(111)_{Al5.72Fe2}$ are as follows: u = 22.284 Å, v = 17.079Å, θ = 57.611°. As the mismatch between $Al_{12.48}Fe_{6.52}$ $(0\bar{1}\bar{2})$ surface and $Al_{5.72}Fe_2$ (111) surface is very large in the *u* and *v* directions. It is necessary to build a model of the supercell interface to satisfy the periodic boundary conditions. Since it is difficult to eliminate the mismatch in the *u* and *v* directions when constructing very large supercells, relatively small mismatches can be constructed by 5 (*u*)

× 7 (*v*) $(0\bar{1}\bar{2})$ $Al_{12.48}Fe_{6.52}$ and 4 (*u*) × 2 (*v*) (111) $Al_{5.72}Fe_2$ surface models. The mismatches in the *u* and *v* directions of the two surfaces are δ (*u*) = 0.804% and δ (*v*) = 0.468%, respectively. The lattice parameters of $Al_{12.48}Fe_{6.52}$ and $Al_{5.72}Fe_2$ on both sides of the interface are averaged by applying a certain strain to eliminate the two-phase lattice parameters of the interface. The atomic interface model of $Al_{12.48}Fe_{6.52}(0\bar{1}\bar{2})/Al_{5.72}Fe_2(111)$ is shown in Figure 10c, red dot lines represent the dividing line between the $Al_{12.48}Fe_{6.52}$ $(0\bar{1}\bar{2})$ surface and $Al_{5.72}Fe_2$ (111) surface. It can be seen that the atomic arrangement law on the surface of $Al_{12.48}Fe_{6.52}(0\bar{1}\bar{2})$ is that two layers of Fe atoms and one layer of Al atoms are alternately arranged, and the atomic arrangement law on the surface of $Al_{5.72}Fe_2(111)$ is that one layer of Al atoms and one layer of Fe atoms are alternately arranged.

Table 5. Orientation relationships and corresponding conversion matrices between $Al_{12.48}Fe_{6.52}$ and $Al_{5.72}Fe_2$ interfaces.

	Orientation Relationship	Conversion Matrix B	Conversion Matrix A
OR1	$(0\bar{1}\bar{2})$ $Al_{12.48}Fe_{6.52}$//(111) $Al_{5.72}Fe_2$ [100] $Al_{12.48}Fe_{6.52}$//$[\bar{2}11]$ $Al_{5.72}Fe_2$	$\begin{pmatrix} 1.60 & -0.34 & 0.44 \\ -0.44 & -0.93 & 0.06 \\ -0.24 & 0.01 & -0.48 \end{pmatrix}$	$\begin{pmatrix} 0.65 & -0.32 & -0.32 \\ -0.23 & -0.97 & 0.09 \\ 0.57 & -0.41 & -2.37 \end{pmatrix}$
OR2	(308) $Al_{12.48}Fe_{6.52}$//$(\bar{7}30)$ $Al_{5.72}Fe_2$ [010] Al_2Fe//$[\bar{3}726]$ $Al_{5.72}Fe_2$	$\begin{pmatrix} -1.23 & 0.76 & 0.35 \\ 0.38 & -0.40 & 0.57 \\ -0.39 & -0.65 & -0.13 \end{pmatrix}$	$\begin{pmatrix} -0.54 & 0.22 & 0.51 \\ 0.16 & -0.35 & 1.39 \\ -0.73 & -1.06 & -0.26 \end{pmatrix}$
OR3	(350) $Al_{12.48}Fe_{6.52}$//$(\bar{4}42)$ $Al_{5.72}Fe_2$ [001] $Al_{12.48}Fe_{6.52}$//[794] $Al_{5.72}Fe_2$	$\begin{pmatrix} 0.10 & 0.33 & -0.90 \\ -0.87 & 0.61 & 0.14 \\ 0.61 & 0.43 & 0.25 \end{pmatrix}$	$\begin{pmatrix} 0.12 & 0.38 & -0.96 \\ -0.60 & 0.74 & 0.20 \\ 0.76 & 0.98 & 0.44 \end{pmatrix}$
OR4	(313) $Al_{12.48}Fe_{6.52}$//$(\bar{5}10)$ $Al_{5.72}Fe_2$ $[\bar{5}92]$ $Al_{12.48}Fe_{6.52}$//[001] $Al_{5.72}Fe_2$	$\begin{pmatrix} -1.14 & 0.83 & 0.38 \\ -0.04 & 0.35 & -0.61 \\ -0.45 & -0.63 & -0.15 \end{pmatrix}$	$\begin{pmatrix} -0.55 & 0.35 & 0.23 \\ -0.15 & 0.43 & -1.38 \\ -0.81 & -0.90 & -0.46 \end{pmatrix}$

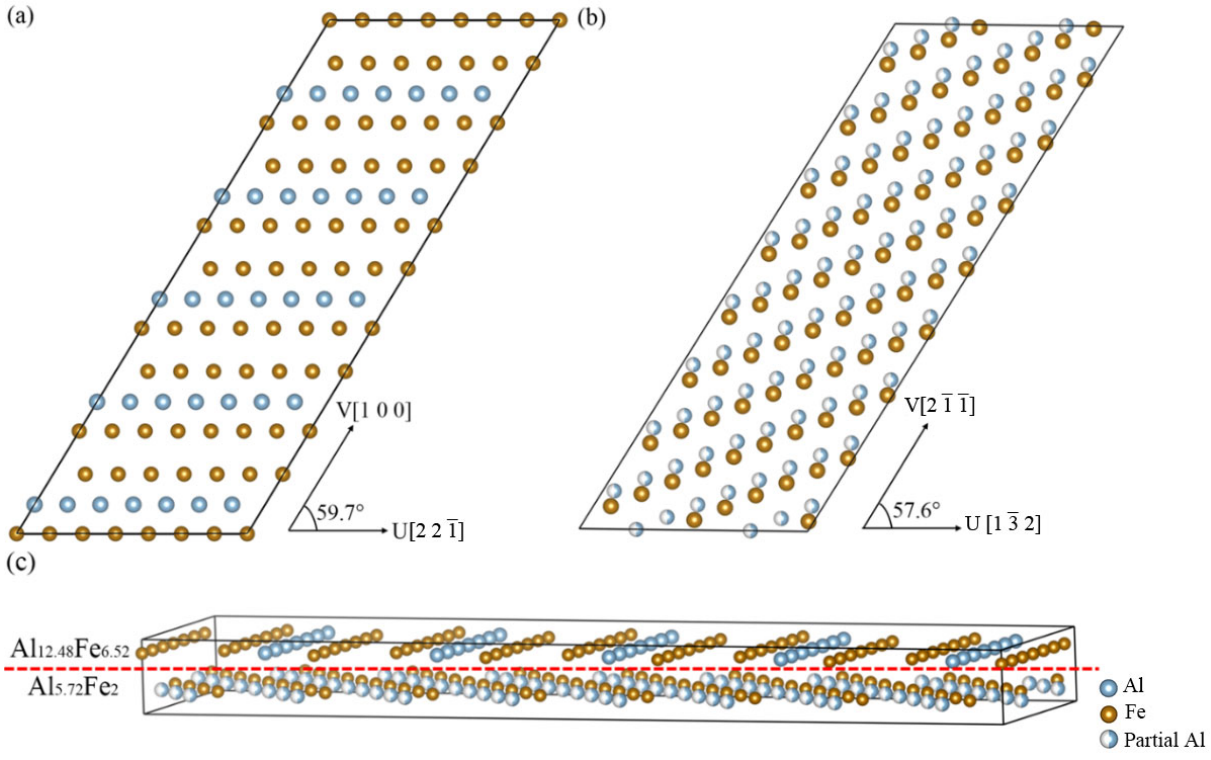

Figure 10. (**a**): $Al_{12.48}Fe_{6.52}$ $(0\bar{1}\bar{2})$ surface; (**b**): $Al_{5.72}Fe_2$ (111) surface; (**c**): the atomic interface model of $Al_{12.48}Fe_{6.52}$ $(0\bar{1}\bar{2})/Al_{5.72}Fe_2$.

4. Conclusions

In summary, two typical phases, $Al_{12.48}Fe_{6.52}$ and $Al_{5.72}Fe_2$ in the Al-Fe, are discovered to be co-existence in the form of single crystals with size of tens of micromeres, which has been confirmed by SXRD by combing SEM/EDX analysis. The first phase, known as Al_2Fe, is refined to be $Al_{12.48}Fe_{6.52}$ (space group $P\bar{1}$) with cell parameters: a = 4.8569 (5) Å, b = 6.4389 (7) Å, c = 8.7323 (10) Å, α = 87.873 (4)°, β = 74.463 (4)°, γ = 83.060 (4)°. There are two co-occupying atoms, namely Fe4A and Al4B, with S.O.F refined to be 0.758 and 0.242, respectively, in accordance with the previously refined model $Al_{12.59}Fe_{6.41}$ determined in 2010. The second phase known as Al_5Fe_2 is refined to be $Al_{5.72}Fe_2$ (space group *Cmcm*) with cell parameters: a = 7.635 (3) Å, b = 6.392 (2) Å, c = 4.2007 (10) Å, $\alpha = \beta = \gamma = 90°$. There are two vacancy atoms, namely Al1 and Al2, with S.O.F refined to be 0.5 and 0.18, respectively. Meanwhile, topological analysis reveals that both phases are composed of 4–8 twisted icosahedrons as structural building units.

Furthermore, crystal structure models for intergrowth $Al_{12.48}Fe_{6.52}$ and $Al_{5.72}Fe_2$ phases have been obtained from the SXRD data sets in reciprocal space as well as the refined model in real space. It needs to be emphasized that the angle between the crystal plane of $Al_{12.48}Fe_{6.52}$ (001) and the crystal plane of $Al_{5.72}Fe_2$ (100) is 63.35°.

Finally, the orientation relationships of interfaces between the two phases are obtained by investigating the synthesized precession planes from the SXRD data sets. Three orientation relationships named OR1, OR2, OR3, and one named OR4 have been obtained by analyzing the (0kl), (h0l), and (hk0) planes of the $Al_{12.48}Fe_{6.52}$ phase and the (hk0) planes of the $Al_{5.72}Fe_2$ phase, respectively. The arrangement of atoms inside the interfaces has been illustrated in a preliminary interface model by taking OR1 as an example.

The present works report a protocol for analyzing the detailed crystal structures of double intergrowth phases and investigating their orientation relationships of interfaces between intergrowth phases, which provide an alternative approach for such investigations besides advanced transmission electron microscopy (TEM) [6,7,20,21] and electron backscattered diffraction (EBSD) techniques [29,30] and will definitely stimulate further related jobs on intergrowth samples which frequently showing up in the complex metallic alloys.

Supplementary Materials: The following supporting information can be downloaded at https://www.mdpi.com/article/10.3390/met14030337/s1. Phi360 diffraction pattern, SEM and EDX analysis of the single-crystal sample, structural relationships between the parent η-Fe_2Al_5, Al-rich low-temperature η′-Fe_3Al_8, and Fe-rich low-temperature η″-Fe_3Al_{7+x} phases [14] and the precession images of the (1*kl*), (*h*1*l*) and (*hk*1) planes-(5*kl*), (*h*5*l*) and (*hk*5) planes can be found in the Supplementary Materials, Figure S1: (a) The Phi360 diffraction pattern collected in the process of single-crystal testing, (b) the powder diffraction pattern obtained by integrating the Phi360 diffraction pattern; Figure S2: Scanning Electron Microscope (SEM) micrographs of single-crystal sample. EDX analysis was performed on different sites corresponding to those listed in Table S1. Table S1: EDX component analysis at each scanning spot; Table S2: EDX component analysis at each scanning spot and area; Figure S3: Scanning Electron Microscope (SEM) micrographs of single-crystal sample. EDX analysis was performed on different sites corresponding to those listed in Table S2. Figure S4: Structural relationships between the parent η-Fe_2Al_5, Al-rich low-temperature η′-Fe_3Al_8, and Fe-rich low-temperature η″-Fe_3Al_{7+x} phases.; Figure S5: The precession images of intergrowth crystals: (a) $Al_{12.48}Fe_{6.52}$(1*kl*), (b) $Al_{12.48}Fe_{6.52}$(*h*1*l*), (c) $Al_{12.48}Fe_{6.52}$(*hk*1), (d) $Al_{5.72}Fe_2$(1*kl*), (e) $Al_{5.72}Fe_2$(*h*1*l*), (f) $Al_{5.72}Fe_2$(*hk*1); Figure S6: The precession images of intergrowth crystals: (a) $Al_{12.48}Fe_{6.52}$(2*kl*), (b) $Al_{12.48}Fe_{6.52}$(*h*2*l*), (c) $Al_{12.48}Fe_{6.52}$(*hk*2), (d) $Al_{5.72}Fe_2$(2*kl*), (e) $Al_{5.72}Fe_2$(*h*2*l*), (f) $Al_{5.72}Fe_2$(*hk*2); Figure S7: The precession images of intergrowth crystals: (a) $Al_{12.48}Fe_{6.52}$(3*kl*), (b) $Al_{12.48}Fe_{6.52}$(*h*3*l*), (c) $Al_{12.48}Fe_{6.52}$(*hk*3), (d) $Al_{5.72}Fe_2$(3*kl*), (e) $Al_{5.72}Fe_2$(*h*3*l*), (f) $Al_{5.72}Fe_2$(*hk*3); Figure S8: The precession images of intergrowth crystals: (a) $Al_{12.48}Fe_{6.52}$(4*kl*), (b) $Al_{12.48}Fe_{6.52}$(*h*4*l*), (c) $Al_{12.48}Fe_{6.52}$(*hk*4), (d) $Al_{5.72}Fe_2$(4*kl*), (e) $Al_{5.72}Fe_2$(*h*4*l*), (f) $Al_{5.72}Fe_2$(*hk*4); Figure S9: The precession images of intergrowth crystals: (a) $Al_{12.48}Fe_{6.52}$(5*kl*), (b) $Al_{12.48}Fe_{6.52}$(*h*5*l*), (c) $Al_{12.48}Fe_{6.52}$(*hk*5), (d) $Al_{5.72}Fe_2$(5*kl*), (e) $Al_{5.72}Fe_2$(*h*5*l*), (f) $Al_{5.72}Fe_2$(*hk*5).

Author Contributions: Conceptualization, B.W., R.F. and L.Z.; methodology, C.F.; investigation, Y.L. and Z.X.; resources, C.F. and Z.X.; writing—original draft preparation, Y.L.; writing—review and

editing, C.F.; writing—review, B.W., Z.X., R.F. and L.Z.; supervision, C.F.; funding acquisition, C.F. All authors have read and agreed to the published version of the manuscript.

Funding: This research was funded by National Natural Science Foundation of China (grant No. 52173231; grant No. 51925105), Hebei Natural Science Foundation (grant No. E2022203182; grant No. E2020203158), Project of Hebei Provincial Department of Human Resources and Social Security (grant No. E2020100006), and The Innovation Ability Promotion Project of Hebei supported by Hebei Key Lab for Optimizing Metal Product Technology and Performance (grant No. 22567609H).

Data Availability Statement: The original contributions presented in the study are included in the article/Supplementary Material, further inquiries can be directed to the corresponding author.

Conflicts of Interest: The authors declare that they have no known competing financial interests or personal relationships that could have appeared to influence the work reported in this paper.

Appendix A

During data processing, the orientation matrix is a 3 × 3 matrix, which specifies the component values and orientations of the three reciprocal axes based on the x, y, and z coordinates on the goniometer. This matrix, therefore, contains the basic data that defines the reciprocal cell and its spatial orientation. The orientation matrix in reciprocal space can be described as:

$$\mathrm{R} = \begin{pmatrix} a_x^* & b_x^* & c_x^* \\ a_y^* & b_y^* & c_y^* \\ a_z^* & b_z^* & c_z^* \end{pmatrix} \tag{A1}$$

a^* corresponds to the first column, b^* to the second, c^* to the third. The subscripts x, y, and z indicate the Cartesian coordinates of the diffractometer.

The orientation matrix of $Al_{12.48}Fe_{6.52}$ phase and $Al_{5.72}Fe_2$ phase in reciprocal space is recorded by the APEX3 software, where the orientation matrix of $Al_{12.48}Fe_{6.52}$ phase in reciprocal space is:

$$\begin{pmatrix} +0.13465488 & +0.02485142 & -0.10581445 \\ -0.09946004 & -0.09375799 & -0.05067891 \\ -0.13488966 & +0.12265494 & -0.01804230 \end{pmatrix} \tag{A2}$$

The orientation matrix of the $Al_{5.72}Fe_2$ phase in reciprocal space is:

$$\begin{pmatrix} +0.00026973 & +0.15365113 & +0.04200600 \\ +0.10967476 & -0.01534700 & +0.12811274 \\ +0.07172056 & +0.02289071 & -0.19606741 \end{pmatrix} \tag{A3}$$

From the basic correspondence between reciprocal space and real space [28]:

$$a^* \cdot a = b^* \cdot b = c^* \cdot c = 1 \tag{A4}$$

One can derive the orientation matrix of these two phases in real space. Where the orientation matrix of $Al_{12.48}Fe_{6.52}$ phase in real space is:

$$\begin{pmatrix} +2.07050255 & -3.28088174 & -2.92743045 \\ +1.32006580 & -4.37338517 & +4.54245615 \\ -6.50564472 & -5.20223437 & -2.65848672 \end{pmatrix} \tag{A5}$$

The orientation matrix of the $Al_{5.72}Fe_2$ phase in real space is:

$$\begin{pmatrix} +0.01570701 & +6.38666400 & +4.17648610 \\ +6.30539906 & -0.62979677 & +0.93936868 \\ +0.74189574 & +2.26268416 & -3.46287667 \end{pmatrix} \tag{A6}$$

Through the orientation matrix of $Al_{12.48}Fe_{6.52}$ and $Al_{5.72}Fe_2$ phases in real space, the comprehensive models of $Al_{12.48}Fe_{6.52}$ and $Al_{5.72}Fe_2$ described with cell edges in real space can be constructed, as shown in Figure 8a of the main text.

Now, we can add the specific atoms for both phases to the orientation models described with cell edges by acknowledging the experimental orientation matrix and the Crystallographic Information File (CIF) related orientation matrix. First, the positions of atoms of the $Al_{5.72}Fe_2$ phase in real space are introduced. We named the experimental orientation matrix of the phase in the real space as matrix B. The CIF-related orientation matrix corresponding to $Al_{5.72}Fe_2$ is described as:

$$\mathrm{A} = \begin{pmatrix} 7.63500 & 0 & 0 \\ 0 & 6.39200 & 0 \\ 0 & 0 & 4.20070 \end{pmatrix} \tag{A7}$$

Based on matrix A and matrix B, one can find the transformation relationship between the two matrices, let AC = B, Then the matrix C is:

$$\mathrm{C} = \begin{pmatrix} +0.00205724 & +0.83649824 & +0.54701848 \\ +0.98645169 & -0.09852891 & +0.14696007 \\ +0.17661241 & +0.53864454 & -0.82435704 \end{pmatrix} \tag{A8}$$

Then, the cartesian coordinates of the atoms in the CIF of $Al_{5.72}Fe_2$ are multiplied by the matrix C, resulting in the coordinate positions of the atoms of the $Al_{5.72}Fe_2$ phase in real space. Second, the coordinate positions of the atoms of the $Al_{12.48}Fe_{6.52}$ phase in real space are also obtained in the same way. Finally, the comprehensive oriented structural models of $Al_{12.48}Fe_{6.52}$ and $Al_{5.72}Fe_2$ phases in real space are obtained, as shown in Figure 8b of the main text.

Appendix B

The matrix method is to find out the conversion relationship between the crystal plane index and the crystal direction index between two phases mathematically, i.e., to find the transformation matrix B and A of each kind of orientation relation. If the absolute values of the nine elements in the transformation matrix are identical, it can be judged that the orientation relation of the two phases belongs to the same type even though the positive/negative signs and the arrangement order and position are different. The crystal plane (*hkl*) can be represented by a reciprocal vector in the reciprocal space. $G^*_{hkl}(=ha^*_1 + ka^*_2 + la^*_3)$. The normal direction of the crystal plane (*hkl*) is the positive vector and can be expressed $I_{uvw}(=ua_1 + va_2 + wa_3)$. The relationship between $G^*_{hkl}(=ha^*_1 + ka^*_2 + la^*_3)$ and $I_{uvw}(=ua_1 + va_2 + wa_3)$ is as follows:

$$\begin{bmatrix} h \\ \mathrm{k} \\ \mathrm{l} \end{bmatrix} = \mathrm{G} \begin{bmatrix} \mathrm{u} \\ \mathrm{v} \\ \mathrm{w} \end{bmatrix} \tag{A9}$$

$$\begin{bmatrix} u \\ v \\ \mathrm{w} \end{bmatrix} = \mathrm{G}^{-1} - \begin{bmatrix} \mathrm{h} \\ \mathrm{k} \\ \mathrm{l} \end{bmatrix} \tag{A10}$$

Among them, for any crystal system, there are:

$$\mathrm{G} = \begin{bmatrix} a^2 & ab\cos\gamma & ac\cos\beta \\ ab\cos\gamma & b^2 & bc\cos\alpha \\ ac\cos\beta & bc\cos\alpha & c^2 \end{bmatrix} \tag{A11}$$

where a, b, c, α, β, γ are the lattice parameters.

In the general crystallographic study, the orientation relationship between two phases is always expressed in the form of $[u_2'v_2'w_2']//[u_2v_2w_2]$, $(h_1'k_1'l_1')//(h_1k_1l_1)$. The second group of crystal plane parallelism $(h_2'k_2'l_2')//(h_2k_2l_2)$ can be obtained according to the crystal direction parallelism and Formula (A9). According to $(h_1'k_1'l_1')//(h_1k_1l_1)$ and Formula (A10), one can obtain the second crystal orientation parallel relationship $[u_1'v_1'w_1']//[u_1v_1w_1]$. Then the $(h_3'k_3'l_3')$ can be obtained by $[u_1'v_1'w_1'] \times [u_2'v_2'w_2']$, the $(h_3k_3l_3)$ can be obtained by $[u_1v_1w_1] \times [u_2v_2w_2]$. Therefore, three groups of crystal plane parallelism between the two phases can be obtained.

$$\begin{cases} (h_1'k_1'l_1')//(h_1k_1l_1) \\ (h_2'k_2'l_2')//(h_2k_2l_2) \\ (h_3'k_3'l_3')//(h_3k_3l_3) \end{cases} \tag{A12}$$

The above orientation relationship can be expressed in the following matrix form:

$$\begin{bmatrix} u' \\ v' \\ w' \end{bmatrix} = B \begin{bmatrix} u \\ v \\ w \end{bmatrix}, \quad \begin{bmatrix} h' \\ k' \\ l' \end{bmatrix} = A \begin{bmatrix} h \\ k \\ l \end{bmatrix} \tag{A13}$$

where B is the conversion matrix, A and B are transposed inverse matrices of each other, and the expression of the conversion matrix B is as follows:

$$B = \begin{bmatrix} h_1' & k_1' & l_1' \\ h_2' & k_2' & l_2' \\ h_3' & k_3' & l_3' \end{bmatrix}^{-1} \begin{bmatrix} \frac{d_1}{d_1'} & 0 & 0 \\ 0 & \frac{d_2}{d_2'} & 0 \\ 0 & 0 & \frac{d_3}{d_3'} \end{bmatrix} \begin{bmatrix} h_1 & k_1 & l_1 \\ h_2 & k_2 & l_2 \\ h_3 & k_3 & l_3 \end{bmatrix} \tag{A14}$$

where d_1, d_2, d_3 are the interplanar spacing of $(h_1k_1l_1)$, $(h_2k_2l_2)$ and $(h_3k_3l_3)$; d_1', d_2', d_3' are the interplanar spacing of $(h_1'k_1'l_1')$, $(h_2'k_2'l_2')$ and $(h_3'k_3'l_3')$.

For the $Al_{12.48}Fe_{6.52}/Al_{5.72}Fe_2$ phase interfaces reported in the present work, when substituting the lattice constants of these two phases into the formula, the crystal-to-plane conversion matrix of $Al_{12.48}Fe_{6.52}$ and $Al_{5.72}Fe_2$ can be obtained as follows:

$$GAl_{12.48}Fe_{6.52} = \begin{bmatrix} 23.590 & 3.779 & 11.360 \\ 3.779 & 41.460 & 2.122 \\ 11.360 & 2.122 & 76.253 \end{bmatrix} \tag{A15}$$

$$GAl_{5.72}Fe_2 = \begin{bmatrix} 58.293 & 0 & 0 \\ 0 & 40.858 & 0 \\ 0 & 0 & 17.646 \end{bmatrix} \tag{A16}$$

References

1. Fung, K.K.; Yang, C.Y.; Zhou, Y.Q.; Zhao, J.G.; Zhan, W.S.; Shen, B.G. Icosahedrally related decagonal quasicrystal in rapidly cooled Al-14-at.%-Fe alloy. *Phys. Rev. Lett.* **1986**, *56*, 2060–2063. [CrossRef]
2. Shechtman, D.; Blech, I.; Gratias, D.; Cahn, J.W. Metallic phase with long-range orientational order and no translational symmetry. *Phys. Rev. Lett.* **1984**, *53*, 1951–1953. [CrossRef]
3. Hamada, T.; Higashi, M.; Niitsu, K.; Inui, H. Phase equilibria among η-Fe_2Al_5 and its higher-ordered phases. *Sci. Technol. Adv. Mater.* **2021**, *22*, 373–385. [CrossRef]
4. Khalid, M.Z.; Friis, J.; Ninive, P.H.; Marthinsen, K.; Ringdalen, I.G.; Strandlie, A. First-principles study of tensile and shear strength of an $Fe_2Al_5//Fe$ interface. *Comput. Mater. Sci.* **2021**, *192*, 110319. [CrossRef]
5. Becker, H.; Hielscher, R.; Leineweber, A. Interplay between Habit Plane and Orientation Relationship in an Electron Backscatter Diffraction Analysis: Using the Example of η′-Al_8Fe_3 in η-Al_5Fe_2. *Crystals* **2022**, *12*, 813. [CrossRef]
6. Krisam, S.; Becker, H.; Silvayeh, Z.; Treichel, A.; Domitner, J.; Povoden-Karadeniz, E. Formation of long-range ordered intermetallic η‴phase and the involvement of silicon during welding of aluminum-steel sheets. *Mater. Charact.* **2022**, *187*, 111862. [CrossRef]
7. Liao, H.; Mo, L.; Zhou, X.; Yuan, Z.; Du, J. Revealing the nucleation event of Mg-Al alloy induced by Fe impurity. *Int. J. Min. Met. Mater.* **2022**, *29*, 1317–1321. [CrossRef]
8. Corby, R.N.; Black, P.J. The structure of $FeAl_2$ by anomalous dispersion methods. *Acta Crystallogr. Sect. B Struct. Crystallogr. Cryst. Chem.* **1973**, *29*, 2669–2677. [CrossRef]

9. Bastin, G.F.; Van Loo, F.J.J.; Vrolijk, J.W.G.A.; Wolff, L.R. Crystallography of aligned Fe-Al eutectoid. *J. Cryst. Growth* **1978**, *43*, 745–751. [CrossRef]
10. Chumak, I.; Richter, K.W.; Ehrenberg, H. Redetermination of iron dialuminide, $FeAl_2$. *Acta Crystallogr. Sect. C Cryst. Struct. Commun.* **2010**, *66*, i87–i88. [CrossRef] [PubMed]
11. Schubert, K.; Rösler, U.; Kluge, M.; Anderko, K.; Härle, L. Kristallographische ergebnisse an phasen mit durchdringungsbindung. *Sci. Nat.* **1953**, *40*, 437. [CrossRef]
12. Burkhard, U.; Grin, Y.; Ellner, M.; Peters, K. Structure refinement of the iron—Aluminium phase with the approximate composition Fe_2Al_5. *Acta Crystallogr. Sect. B Struct. Sci.* **1994**, *50*, 313–316. [CrossRef]
13. Becker, H.; Leineweber, A. Atomic channel occupation in disordered η-Al_5Fe_2 and in two of its low-temperatures phases, η″ and η‴. *Intermetallics* **2018**, *93*, 251–262. [CrossRef]
14. Okamoto, N.L.; Higashi, M.; Inui, H. Crystal structure of η″-Fe_3Al_{7+x} determined by single-crystal synchrotron X-ray diffraction combined with scanning transmission electron microscopy. *Sci. Technol. Adv. Mater.* **2019**, *20*, 543–556. [CrossRef] [PubMed]
15. Okamoto, N.L.; Okumura, J.; Higashi, M.; Inui, H. Crystal structure of η′-Fe_3Al_8; low-temperature phase of η-Fe_2Al_5 accompanied by an ordered arrangement of Al atoms of full occupancy in the c-axis chain sites. *Acta Mater.* **2017**, *129*, 290–299. [CrossRef]
16. Becker, H.; Amirkhanyan, L.; Kortus, J.; Leineweber, A. Powder-X-ray diffraction analysis of the crystal structure of the η′-Al_8Fe_3 (η′-$Al_{2.67}Fe$) phase. *J. Alloys Compd.* **2017**, *721*, 691–696. [CrossRef]
17. Mihalkovič, M.; Widom, M. Structure and stability of Al_2Fe and Al_5Fe_2: First-principles total energy and phonon calculations. *Phys. Rev. B.* **2012**, *85*, 014113. [CrossRef]
18. Hirata, A.; Mori, Y.; Ishimaru, M.; Koyama, Y. Role of the triclinic Al_2Fe structure in the formation of the Al_5Fe_2-approximant. *Philos. Mag. Lett.* **2008**, *88*, 491–500. [CrossRef]
19. Romero-Romero, J.R.; López-Miranda, J.L.; Esparza, R.; Espinosa-Medina, M.A.; Rosas, G. High-energy ball-milling of $FeAl_2$ and Fe_2Al_5 intermetallic systems. *Mater. Sci. Forum.* **2013**, *755*, 47–52. [CrossRef]
20. Liu, Y.; Liu, R.; Liu, B.; Zhu, Z.; Li, Y.; Chen, H. Interface characterization and tensile performance of deep-penetration welding-brazing of thick aluminium/steel butt joints. *Mater. Charact.* **2022**, *186*, 111811. [CrossRef]
21. Li, R.; Li, T.; Xu, J.; Ding, H. A novel amorphous-nanocrystalline interface layer for bonding immiscible Mg/steel by pinless friction stir spot weld with preset nanoscale Fe_2Al_5 film. *Mater. Charact.* **2023**, *203*, 113092. [CrossRef]
22. *APEX3, SAINT and SADABS; Software for Data Reduction, Absorption Correction and Structure Solution*; Bruker AXS Inc.: Madison, WI, USA, 2015.
23. Krause, L.; Herbst-Irmer, R.; Sheldrick, G.M.; Stalke, D. Comparison of silver and molybdenum microfocus X-ray sources for single-crystal structure determination. *J. Appl. Crystallogr.* **2015**, *48*, 3–10. [CrossRef]
24. Sheldrick, G.M. Crystal structure refinement with SHELXL. *Acta Crystallogr. C Struct. Chem.* **2015**, *71*, 3–8. [CrossRef] [PubMed]
25. Sheldrick, G.M. SHELXT–Integrated space-group and crystal-structure determination. *Acta Crystallogr. A Found Adv.* **2015**, *71*, 3–8. [CrossRef] [PubMed]
26. Putz, H.; Brandenburg, K. Diamond 4.2.2 Crystal and Molecular Structure Visualization. *Crystal. Impact Kreuzherrenstr.* **2017**, *102*, 53227.
27. Blatov, V.A.; Shevchenko, A.P.; Proserpio, D.M. Applied topological analysis of crystal structures with the program package ToposPro. *Cryst. Growth Des.* **2014**, *14*, 3576–3586. [CrossRef]
28. Aroyo. *M.-I. International Tables for Crystallography Vol.A: Space-Group Symmetry*; International Union of Crystallography: Chester, UK, 2016; pp. 22–28.
29. Lobanov, M.L.; Zorina, M.A.; Reznik, P.L.; Redikultsev, A.A.; Pastukhov, V.I.; Karabanalov, M.S. Crystallography of Recrystallization in Al and Cu with Fiber Texture. *Metals* **2023**, *13*, 1639. [CrossRef]
30. Yang, H.; Zhang, Y.; Zhang, A.; Stein, F.; Xu, Z.; Tang, Z.; Ren, D.; Zeng, J. The Mechanism of Dendrite Formation in a Solid-State Transformation of High Aluminum Fe-Al Alloys. *Materials* **2023**, *16*, 2691. [CrossRef]